Polymer 50 (2009) 4964–4972

Contents lists available at ScienceDirect

Polymer

journal homepage: www.elsevier.com/locate/polymer

Microstructures of lamella-forming diblock copolymer melts under nanorod-array confinements

Xianghong Wang [a], Shiben Li [b], Peng Chen [c], Linxi Zhang [b,*], Haojun Liang [d]

[a] Department of Physics, Zhejiang University, Hangzhou, Zhejiang 310027, China
[b] Department of Physics, Wenzhou University, Wenzhou, Zhejiang 325035, China
[c] School of Chemistry, Anhui University, Hefei, Anhui 230039, China
[d] Department of Polymer Science and Engineering, University of Science and Technology of China, Hefei, Anhui 230026, China

ARTICLE INFO

Article history:
Received 5 July 2009
Received in revised form
3 August 2009
Accepted 6 August 2009
Available online 12 August 2009

Keywords:
Microstructure
Nanorod-array confinement
Self-consistent field theory

ABSTRACT

The microstructures of lamellae-forming diblock copolymer melts confined in nanorod arrays are investigated using the real-space self-consistent field theory. The nanorod array leads to the incomplete confinement at each direction so that the confinement-dimension is fractional between zero and two. This incomplete confinement can yield a rich variety of mixture microstructures by varying its fractional confinement-dimension, such as the mixture of concentric lamellae and parallel lamellae and the mixture of the concentric lamellae and cylinders, as well as a series of continuous network mixtures. By comparing with the available simulations and experiments, these novel microstructures can be understood based on the symmetry competition and structural frustration that originated from the incomplete confinement. Our theoretical predictions may be helpful to the design of nanomaterials.

1. Introduction

Designing microstructures is of current interest for various applications including lithography, photonic crystals and laser devices [1–3]. For example, the PS-*b*-PI diblock copolymers have been utilized as a narrow spectral-band selective feedback element to construct a laser cavity, in which the optically pumped surface-emitting lasing action has been demonstrated [3]. This block copolymer-based microstructure opens the possibility of creating the fast and low-cost processing laser devices. Usually, two approaches are used to explore the novel block copolymer-based microstructures. One approach is to search the phase parameter space over a wide range in detail, and the other is to introduce the confinement surface into the block copolymer system. When a geometric surface is introduced into the system of block copolymers, the confinement surface breaks the bulk balance through reorganizing the microstructures to meet the minimization of free energy. The confinement-induced microstructure depends not only on the volume fraction of block and block repulsion interactions between the different blocks but also on the shape and curve of confinement surface [4]. Therefore, The geometric confinement has been proven to be an efficient approach to produce the microstructures of block copolymers in the process of self-assembly [4,5].

To explore the novel microstructures, several types of confinements, such as the thin film (one-dimensional) confinement, the cylindrical nanopore (two-dimensional) confinement and the spherical cavity (three-dimensional) confinement, have been employed to study their different confinement effects on the block copolymer systems. It is demonstrated that the integral confinement dimension plays an important role in the confined self-assembly due to their different symmetries of the confinement surfaces. Specifically, when the lamella-forming diblock copolymers are under one-dimensional (1D) confinement, the thin film confinement, the lamella thickness can be compressed or stretched, and even the lamellae are oriented normal to the film surface without changing their bulk period [6–14]. Unlike the 1D film-confinement case where the lamella maintains the flat characteristic, the 2D nanopore-confinement requires the curving structures for the lamella-forming diblock copolymers [15]. Many studies revealed that the lamella structures can accommodate themselves to the confinement shape so that the cylindrically concentric lamellae (CL) can be observed under the nanopore confinements [16–23]. Furthermore, the CL structure has been quantitatively analyzed by the Monte Carlo (MC) simulation and the strong stretching theory (SST) for the diblock copolymers in the strong segregation region [21,22]. Many other types of curving structures, such as the single helix and the double helix structures, have also been obtained as the confinement degree is suitable [15,17,18,21,23]. For the 3D spherical confinement, the bulk lamellae can assemble into the concentric spherical lamellae due to the

* Corresponding author. Tel.: +86 571 88483790; fax: +86 571 87951328.
E-mail address: lxzhang@zju.edu.cn (L. Zhang).

0032-3861/$ – see front matter © 2009 Elsevier Ltd. All rights reserved.
doi:10.1016/j.polymer.2009.08.009

spherical symmetry in the presence of surface field [24,25]. Furthermore, the thickness of concentric spherical lamellae has also been analyzed by the SST, which is in good agreement with the MC results [25]. Recently, the experimental study reported that a series of frustrated microstructures, such as the screw-like, mushroom and wheel-like structures, have been observed for the diblock copolymers confined in the nanoparticles [26].

The cylinder-forming diblock copolymer melts display the more complicated microstructures because of the hexagonally arranged cylinders that have different symmetries from the confinement symmetry. For instance, the cylinder-forming diblock copolymers can be deformed into a series of microstructures under the 1D thin-film confinement, such as the elliptical cylinders, undulated cylinders, lamellae, undulated lamellae, and perforated lamellae, when the model copolymers are chosen to be located in the intermediate segregation region [27–32]. For the 2D nanopore-confinement, the hexagonally arranged cylinders can be distorted into a series of frustration structures for the various pore diameters including the single cylinder, stacked disk, single helix, double helix, and so on [21,27,33–36]. Moreover, the pitch angles of helices have been investigated by a simple geometrical argument [34,35]. In particular, Chen et al. have employed the self-consistent theory (SCFT) to discuss the origin of microstructures from the diblock copolymers where the system parameters are selected to be located near the phase boundary [27]. For 3D spherical confinement, the complete confinement in three spatial directions leads to the complicated center-symmetric microstructures when the sphere diameter is increased to a suitable value [37]. Several microstructures from 3D spherical confinements have also been observed in experiment by TEM method, in which the interaction between the polymers and surfaces plays an important role on the self-assembly of microstructures [38].

Although a considerable numbers of literature have contributed to the confinement effects on the microstructures of diblock copolymers, these confinement-dimensions are integers that are independent of the confinement degree. In other words, these confinement systems only provide the unalterable symmetry due to the integer confinement-dimension. Of physical viewpoint, it is interesting to study the confined system with the fractional confinement-dimension. Recently, we have used the SCFT method to investigate the microstructures of the lamella-forming diblock copolymer under the nanorod-array-confinement where a series of microstructures have been observed by varying the fractional confinement-dimension [39]. In our previous work, the period of nanorod array is limited to the bulk polymer period, leading to a high number density of nanorods. This astriction results in the disordered microstructures when the nanorod diameter is increased to be 41% of array period. However, it is important to understand how the confinement-dimension affects the microstructure over a wide range. In the present work, we extend our previous work and vary the fractional confinement-dimension over a wide range to investigate its effects on the microstructures of lamella-forming diblock copolymer. This may deepen the understanding of confinement-induced microstructures for the diblock copolymers, which may be helpful to the microstructure designs. In the next section, we will define the fraction confinement dimension and introduce the calculation method. Then we discuss the main results in the third section, and consider two types of array surfaces, the neutral and preferential surfaces. The conclusions are presented in the last section.

2. Model and method

The diblock copolymers are confined in a nanorod array with the solid and impenetrate surfaces. The nanorod array is composed of the periodically arranged nanorods, having the infinite lengths and the diameters D. Here, the position of nanorods is fixed, which is different from our previous model with the mobile nanorods [40]. In this model, we only consider the fractional confinement-dimension effects on the diblock copolymers other than the effects of copolymers on the nanorods. To illustrate the model conveniently, we plotted the cross section of array in the x–y plane with the period L_x and L_y in the x and y directions, respectively, as shown in Fig. 1. Actually, it is impossible to calculate the data for the whole array because of the limitation of computer capability. Therefore, a calculation unit with the periodic boundary condition (PBC, the zone with red lines) is introduced to construct the infinite size of nanorod array in the simulation. The match between the bulk polymer period and the PBC is crucial to avoid an artifact microstructures in a system of infinite size [11,32]. In this report, we selected the calculation unit size to be suitable multiple of the bulk polymer repeat period L_0, that is, $L_z = 2L_0$ and $L_x = L_y = 3L_0$, in order to meet the PBC match and construct the infinite size of nanorod array. Under these considerations, the array has a relatively low number density of nanorod, which is convenient to adjust the confinement-dimension by varying the rod diameter.

Then, we define confinement-dimension for the nanorod-array-confinement as follows. First, we define the confinement-dimension at each direction, the x and y directions, respectively, as the ratio between projection area of all nanorods and the whole array, namely, $d_x = S'_x/S_x$ and $d_y = S'_x/S_y$, as illustrated in Fig. 1. Secondly, we define the total confinement-dimension as $d = d_x + d_y$ in a straightforward way when the array has the same periods at the x and y directions. Therefore, it is easy to deduce that the confinement-dimension for our model is $d = 2D/L$ since the array has the periods of $L_x = L_y = L$ and the rods have the same diameter D. The definition of confinement-dimension d is different from the

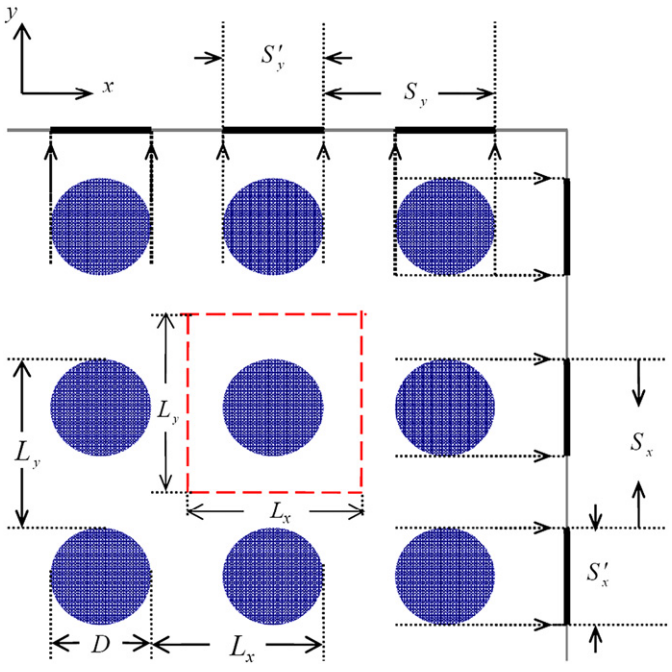

Fig. 1. Sketch map of periodic nanorod array with fractional confinement dimension in the x–y planes. Here, D denotes the diameter of rod, L_x and L_y represent the array periods in the x and y directions, respectively. S_x and S_y represent the projection area of array in the x and y directions while the S'_x and S'_y is the projection area of nanorod in the x and y directions, respectively. The zone with red dotted lines represents the calculation unit. (For interpretation of the references to colour in this figure legend, the reader is referred to the web version of this article.)

confinement degree that described as the ratio between pore diameter and bulk lamella period in the nanopore confinements [21,27]. The interesting characteristic is that the confinement degree only describes the degree for the confined diblock copolymers in the nanopore with a certain cylindrical symmetry, while the fractional confinement-dimension not only involves the confinement degree but also results in the different symmetries. For example, when the rod diameter is reduced to be $D \approx 0$, the confinement-dimension can be expressed as $d \approx 0$. In this case, the confinement can be neglected and the system exhibits the bulk symmetry. When the diameter is increased to be $D = L$, the confinement-dimension is to be $d = 2$. However, we should note that this integral confinement dimension is different from the 2D cylindrical nanopore-confinement. Here, we mainly consider the different effects of confinement-dimension on the microstructures of confined diblock copolymers.

The diblock copolymers confined in the array can be described as Gaussian chains with the volume fraction of A(B) block $f_{A(B)}$, which are regarded as the particles diffused in random ways, according to the Edward's theory. The theoretical calculation begins with the free energy, which can be written as follow [27,31,41]:

$$\frac{F}{nk_BT} = -\ln\left(\frac{Q}{V}\right) + \frac{1}{V}\int dr[\chi N\phi_A\phi_B - \omega_A\phi_A - \omega_B\phi_B + U_A\phi_A + U_B\phi_B - P(\phi_0 - \phi_A - \phi_B)] \quad (1)$$

The free energy per chain is in the unit of k_BT and includes two terms, the logarithmic term and integral term. The first term is an entropy term originated from the chain stretching that determined by the partition function of a single diblock copolymer. This partition function, Q, can be expressed as $Q = \int drq(r, 1)$, where the propagator, q (r, s), denotes the probability of any monomers at position r, and satisfies a modified diffusion equation,

$$\frac{\partial}{\partial s}q(r,s) = R_g^2\nabla^2 q(r,s) - N\omega q(r,s)$$

and

$$\frac{\partial}{\partial s}q'(r,s) = -R_g^2\nabla^2 q'(r,s) + N\omega q'(r,s), \quad (2)$$

with the initial conditions $q(r, 0) = 1$ and $q'(r, 1) = 1$, in which the conjugated propagator $q'(r, s)$ express the diffusion behavior of monomer, representing the diffusion from the other end of polymer chain. Here, R_g is the radius of gyration for an ideal Gaussian chain with the polymerization index N. For the diblock copolymer, when $0 \le s \le f_A$, $\omega = \omega_A$, otherwise $f_A < s \le 1$, $\omega = \omega_B$. In the present work, we used the Crank–Nicholson scheme to solve these two modified diffusion equations, which has been proved to be efficient for the various confinement boundary conditions [27,39,42].

The integral term represents the energy from the blocks interacted with each other in the external fields. The denotation χN is the repulsion interaction strength between the different blocks where χ is the Flory–Huggins parameter. While $\phi_{A(B)}$ is the monomer density field normalized by the local volume fractions of blocks. The external field includes three parts. One is that the self-consistent fields, $\omega_{A(B)}$, from the repulsion interactions between A- and B-blocks. The second is that the pressure field P, ensuring the incompressibility of system. Here, we generalize incompressibility constraint to be $\phi_A + \phi_B = \phi_0$, and simplified $\phi_0 = 0.5$ on the lattices next to the outer surfaces of rods and $\phi_0 = 1$ on the elsewhere except the solid rods (that is, $\phi_0 = 0$). The third is that the surface field, $U_{A(B)}$, which is only applied to the lattices next to the outer surfaces of rods, reflecting the short-range surface-polymer interactions between the nanorod surfaces and A(B) blocks.

At equilibrium, the free energy of system will be minimized to a stable value. This minimization of free energy results in a set of self-consistent equations under the mean field approximation, which is

$$\omega_A(r) = \chi(\phi_B(r) - f_B) + U_A(r) + P(r), \quad (3)$$

$$\omega_B(r) = \chi(\phi_A(r) - f_A) + U_B(r) + P(r), \quad (4)$$

$$\phi_A(r) = \frac{V}{Q}\int_0^{f_A} dsq(r,s)q'(r,s), \quad (5)$$

$$\phi_B(r) = \frac{V}{Q}\int_{f_A}^{1} dsq(r,s)q'(r,s). \quad (6)$$

The self-consistent equations can be numerically solved by the spectral method and the combinatorial screening method, respectively [43,44]. The real-space combinatorial screening method is suitable to explore the novel microstructures of copolymers because it does not require assumptions of the system symmetry, where an iteration process with the step N_s is assumed. The interaction process will be break out when the convergence criterion $\Delta F/nk_BT$, that is the difference between the new free energy and old free energy per chain, is satisfied. In the calculation process, we take the free energy criterion to be $\Delta F/nk_BT < 10^{-11}$. Furthermore, the convergences of free energies in system are examined by testing several lattice sizes. The test results indicate that the free energy can converge to a stable value and the equilibrium structure is not influenced by the lattice size when the lattice size is smaller than 0.3 R_g. Since the more refined lattice size requires the startlingly high capability of computer, we take 0.2 R_g as the lattice size in all calculations, and divide the chain contour length into 200 monomers, which is similar to our previous work [27]. Moreover, to ensure that the exact equilibrium microstructures have been obtained, each minimization process is run for several times using different random initial mean fields ω_A and ω_B. In the present work, we choose the model copolymer to be a slightly asymmetric diblock copolymer with $f_A = 0.4$ and $\chi_{AB}N = 40$ instead of selecting the symmetric diblock copolymer. Furthermore, we performed the SCFT calculation in 2D space to determine the bulk repeat period, which is found to be $L_0 = 4.4R_g$ and similar to our previous work [39]. This choice of model copolymer not only allows us to explore the distinct effects of surface fields on either minority blocks (A-blocks) or majority blocks (B-blocks), but also provides a convenient way to compare the results between the present and previous works.

3. Results and discussion

3.1. The neutral surface case

We consider the diblock copolymers confined in the arrays with neutral surfaces, and investigate their microstructures as a function of confinement-dimension, as shown in Fig. 2. The microstructures are presented in the form of three different colors (red, green and blue), representing the density distributions of the monomers belonging to A block, B block, and the nanorods, respectively. The equilibrium microstructures are arranged as a function of d, in which d varies over the range of $d = 0.00$–2.00 with the step of $\Delta d \approx 0.06$. Furthermore, we investigate the dependence of minimal free energy on the confinement-dimension for the equilibrium state in Fig. 3. In addition, the structure denotations and the relative

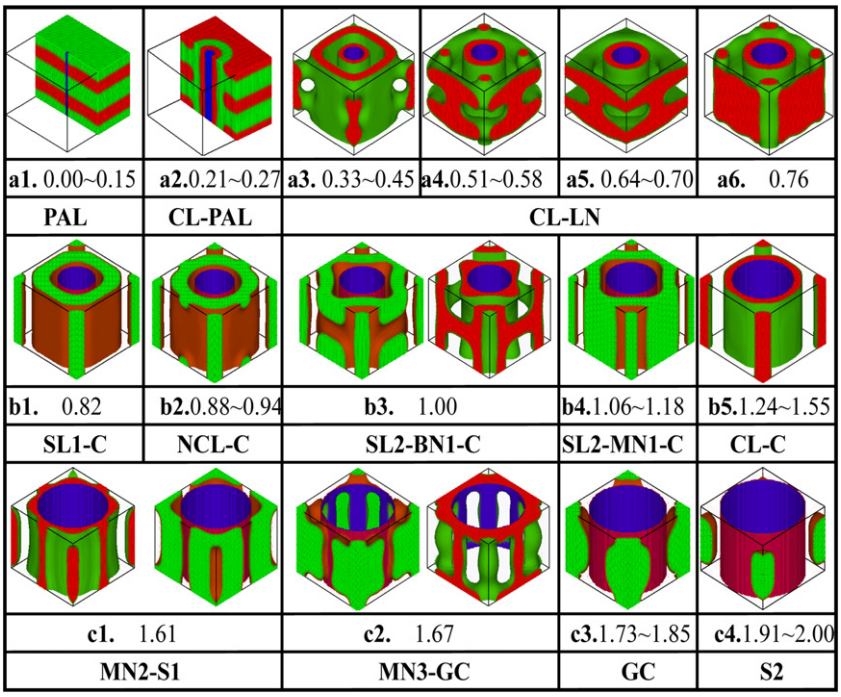

Fig. 2. Dependence of microstructure of lamella-forming diblock copolymers on the confinement-dimension d in the neutral surface case. The red, green, and blue colors represent A-block, B-block, and solid nanorod, respectively (Note that the same form in the following figures). The microstructures are arranged as d where the value of d and the structure denotations are list. (For interpretation of the references to colour in this figure legend, the reader is referred to the web version of this article.)

transitions are illustrated at the proper positions in Figs. 2 and 3, respectively.

For a whole view in Fig. 2, it is an evidence that the confinement-dimension d plays an important role on the microstructure which can be divided into three parts, namely the small, moderate, and large d. For convenience, we divided the microstructures into two zones, the zone near the rod (the inner zone) and the zone away from the rods (the outer zone). Certainly, the diblock copolymers exhibit the bulk structure, the parallel lamellae (PAL), because the effects of confinement-dimension on the microstructures are so weak that they can be ignored at $d = 0.00$–0.15 [Fig. 1.a1]. When the d is increased to be $d = 0.21$–0.27, a monolayer of concentric lamellae (CL) structure is induced in the inner zone due to the cylindrical symmetry about the nanorod while the PAL structure remains in the outer zone, resulting in a CL–PAL mixture structure [Fig. 1.a2]. It is reasonable to deduce that the multilayer CL structures should be observed in the array with the lower number density of nanorod, like the pore-confinement case where the layer number is in proportion to the pore diameter [21]. At $d = 0.33$–0.45, the CL structure with double layers is desired to appear as increasing of d due to the cylindrical symmetry in the inner zone, even though the square symmetry prevails in the outer zone. This symmetric conflict brings on a development of concentric layer into a square layer in the outer zone, and subsequently the square layers connect with the neighboring ones for the other calculation units in the outer zone corners, which results in an irregular lamella network (LN) structure in the outer zones and a CL–LN mixture in the whole array [Fig. 2a3]. Then, we observed an evolvement of LN structure in the outer zone over the range of $d = 0.51$–0.76 [Fig. 2a4–a6]. Namely, the connectivity between the neighboring layers is strengthened with increasing d, which comes into the completely continuity at $d = 0.76$ by passing through a relatively long evolvement process of $d = 0.51$–0.70.

The observations above indicate that the lamella structures dominate in the case of the small d. However, it is not the case for the moderate d where the cylinder structure prevails in the outer zone. Specifically, the C structures appear in the corners of the outer zone and the outer layer of CL structure develops into a square lamella (SL1) in the minority block matrix at $d = 0.82$, due to the square symmetry in the outer zone [Fig. 2.b1]. Therefore, we observed the SL1-C mixture structure. When the d increases, the SL1 structure transits into a partly connected concentric lamella (NCL) structure, leading to the NCL-C mixture structure at $d = 0.88$–0.94 [Fig. 2b2]. At $d = 1.00$–0.55, there is an evolution process for the continuous network structure. This process begins with a bicontinuous network (BN1) structure at $d = 1.00$ where

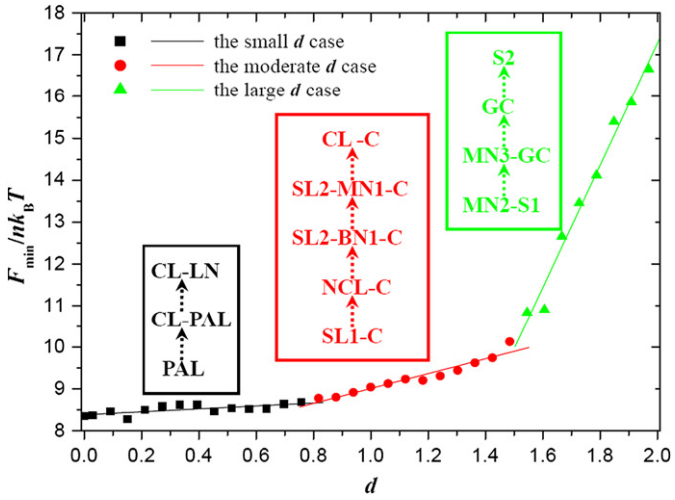

Fig. 3. The dependence of minimal free energy per chain F_{min}/nk_BT on confinement-dimension d. The dots denote the F_{min}/nk_BT for different d, while the simple lines are linear fitting results for the small, moderate and large d, respectively. The structural transitions are also illustrated in the corresponding positions.

either the majority or minority component becomes a continuous network, respectively, as shown in Fig. 2b3. The C structures for the majority blocks and the square lamella (SL2) structures for the minority blocks are separated by this BN1 structure. This SL2-BN1-C mixture structure at $d = 1.00$ is quite different from those structures observed in the thin films with $d = 1.00$ where the microstructures always have the flat characteristics. We believed that the microstructure depends not only on the confinement-dimension but is also determined by the surface curves, and the periodically arrangement for the cylindrical surfaces leads to the above complicated microstructure at $d = 1.00$. For $d = 1.06$–1.18, the majority block components are connected adequately in the outer zone so that the mono-continuous network (MN1) structure occurs accompanying with the increasing layer number for the C structures in the outer zone [Fig. 2b4]. Thus, we observed the SL2-MN1-C mixture structure at $d = 1.06$–1.18. However, the SL2-MN1-C structure continuously transits into the CL-C mixture structure over a wide range of $d = 1.24$–1.55 in the majority block matrix [Fig. 2b5].

For the large d, the relatively small volume restricts the assembly for the most complicated microstructure in the nanorod array. At $d = 1.61$, the cylinder structure transits into a sphere-like (S1) structure in the outer zone, the CL structure connect each other and construct a mono-continuous (MN2) structure in the majority block domain, which is a MN2-S1 mixture structure in the whole array [Fig. 2c1]. Then, the MN2 structure has a slight change and the sphere-like structure disappears in the outer zone at $d = 1.67$, instead of emergence of the generic cylinders (GC) for the majority blocks [Fig. 2c2]. This MN3-GC mixture structure transits into a GC structure at $d = 1.73$–1.85 [Fig. 2c3]. At $d = 1.91$–2.00, the microstructure becomes only the sphere-like (S2) structure for the majority blocks [Fig. 2c4].

Here, we would make several comparisons between the results from the neutral case and the available experiment and simulation. First, we compared the present results to those observed in nanopore-confinement cases. An important phenomenon is that we observed the minority block prefers to the neutral surface on the array-confinement, which is similar to the nanopore-confinement [17,18,21]. Wang et al. called this phenomenon as the hard wall effect and pointed out that this general effect is originate from the entropy effect [45]. It is the hard wall effect that results in the CL structure in the inner zone, similar to the observations on the nanopore-confinement cases. Another general phenomenon is that we observed several discrete structures at the large d including the GC and S structures, like the case where the confinement degree is severe for the nanopore-confinement [15,27]. Then, we compared the present results to our previous work where the array has the high number density of nanorods. The similar results are that both the PAL structures and discrete S structures were observed in these two cases for the weak and severe degrees of d, respectively [39]. However, the more complicated microstructures have been observed in the present study as the d increases because the larger volume provides an enough space to assemble into the complicated microstructures.

In order to investigate structural behaviors in the small, moderate and large d cases, we plotted the curves for the free energies of equilibrium states $F_{\min}/nk_BT$ in Fig. 3, according to Eq. (1). Furthermore, we inserted the structural transition processes in the corresponding positions for handy illustration in Fig. 3. Clearly, there are different trends for the variation of the minimal free energies in these three cases. We used the linear relationships to fit these data and obtained the slopes of $k_1 = 0.348$, $k_2 = 1.775$ and $k_3 = 14.625$ for the small, moderate and large d cases, respectively. The obvious different slopes reflect the different structural transitions in these three cases as d increases. On the one hand, the linear increasing of d in each case indicates that there is not obvious structural transition in the given case. It is clear from illustration that only a part of microstructure changes either in the inner zone or in the outer zone for each case. For example, the structural transition in the small d case is mainly originated from the outer zone while the structure maintains the CL structure in the inner zone. This partly structural transition leads to the smooth change in each case, which is similar to the second-order phase transition. Actually, the second-order phase transition has been observed in the diblock copolymers confined in the thin films where the thickness of PAL structure is changed without changing its orientation [11]. Moreover, the fact of $k_1 < k_2 < k_3$ indicates the different degrees of structural transition in these three cases. Namely, the most drastic structural transition happens in the large d case, in which the diblock copolymers undergo the MN2-S1 to MN3-GC, GC and S2 structures. On the other hand, the first-order structural transition can be observed when the d changes from one case to another case, in which the microstructure exhibits an obvious variation. For instance, the SL-C mixture evolves into the S structure as d is increased from the moderate degree to the large degree. The obvious difference between the slopes of the free energy curve indeed reflects this first-order structural transition happens in the whole process.

3.2. The preferential surface case

The confinement surface not only provides the pure geometric confinement, but can also influences the microstructures by imposing the surface fields. The effects of surface field on the microstructures have been investigated for the diblock copolymers confined in the cylindrical pore [15,20,21,23], spherical cavity [25,37], and even in the array with the fractional d [39]. Here, we selected the strength of surface field to be $U_B = -20$ for the surfaces preferential to the majority blocks in Fig. 4 and $U_A = -40$ for the surfaces preferential to the minority blocks in Fig. 5, respectively. The values of d and the denotations of structures are also list in Figs. 4 and 5. This choice allows us to compare the different effects of surface fields on the majority blocks and minority blocks. Then, we investigated the dependence of entropic energies on the several cylindrical structures in Fig. 6.

We investigated the effects of preferential surfaces on the microstructures of diblock copolymers for the majority blocks, as shown in Fig. 4. We divided the evolvement process into four stages as the d increases, namely $d_1 = 0.00$–0.52, $d_2 = 0.58$–1.00, $d_3 = 1.06$–1.42, and $d_4 = 1.48$–2.00. At the first stage of $d_1 = 0.00$–0.52, the diblock copolymers exhibit the PAL structures over a wide range of $d = 0.00$–0.33 because the surface field is too weak to affect the structures [Fig. 4a1]. In this range, it is the PAL structure instead of the CL–PAL structure that observed in the surfaces preferential to majority blocks. This is because the surface field counteracts the hard wall effect. It is surprising that a frustrated bicontinuous network (BN2) structure was observed at a very narrow range of $d = 0.39$ [Fig. 4a2]. In this microstructure, the minority block component is distorted at a right angle and constructs a continuous microstructure. Meanwhile, the majority block component also forms another continuous microstructure, resulting in the bicontinuous network microstructures, which is similar to our previous results for the array with high number density of nanorods [39]. In the bulk, the BN microstructures can be explained with the minimal interfaces and the symmetry, which are in good agreement with the experiments [46,47]. Actually, the BN microstructure has also been observed in the nanoparticle-polymer composite, in which the particle number density can induce the structural transition [48]. However, the observations here are originated from the structural frustration, the mismatch between the bulk lamella

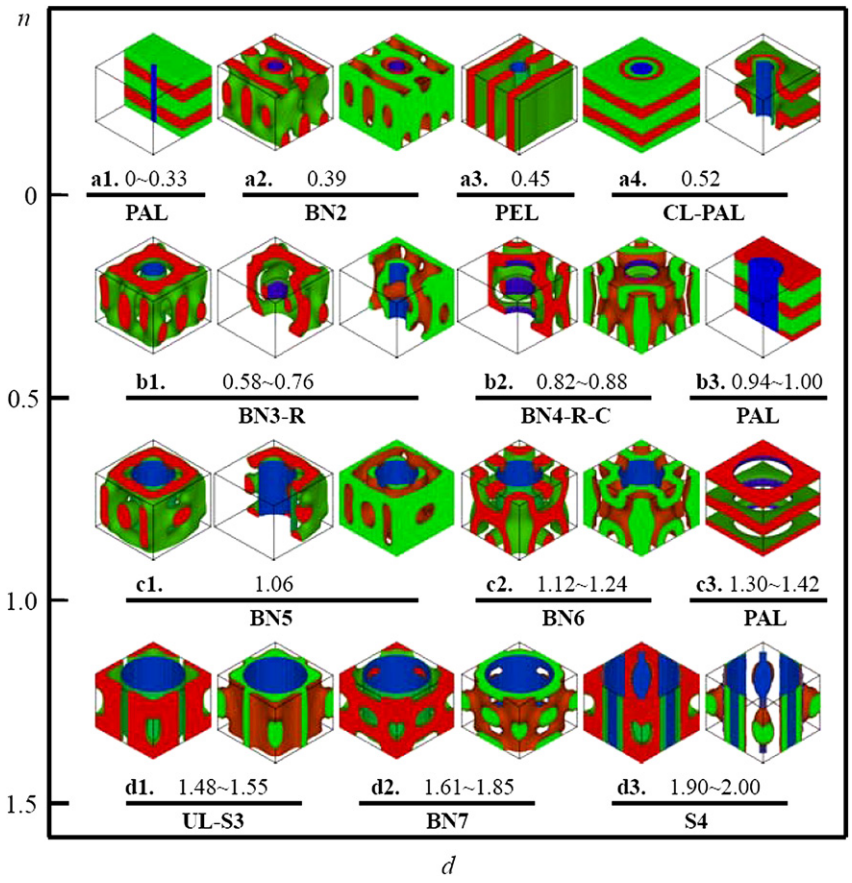

Fig. 4. Dependence of microstructure of lamella-forming diblock copolymers on the confinement-dimension d for the surfaces preferential to the majority blocks. The microstructures are arranged as d where the values of d are list upon the lines and divided into four parts while the structure denotations below the lines. The number n denotes the integer or half integer of d.

period and array confinement. For $d = 0.45$, the bicontinuous network structure evolves into the perpendicular lamellae (PEL) structure [Fig. 4a3]. We note that this PEL structure cannot be observed in the neutral surface case where there are double layers of the concentric cylinder structure at this degree of d, indicating that this phenomenon is mainly due to surface preference instead

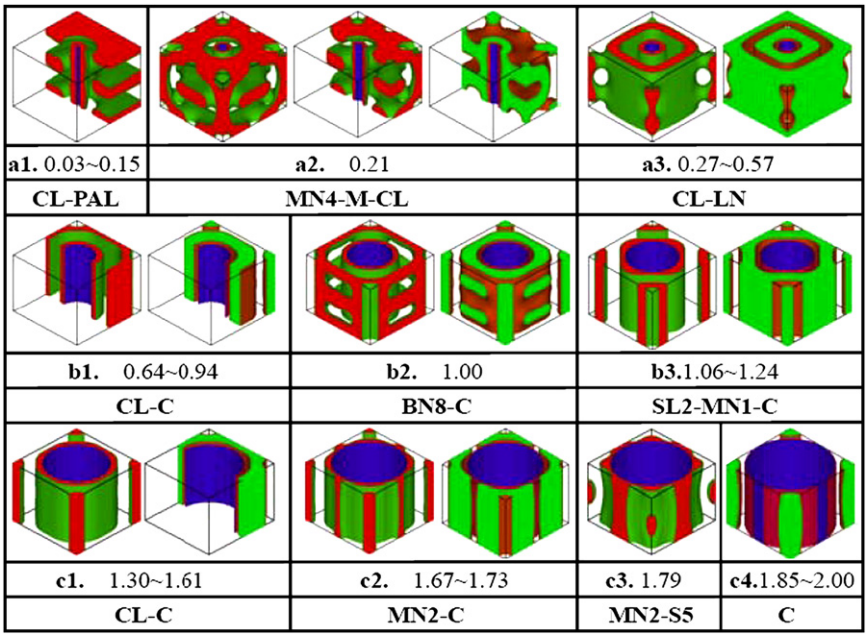

Fig. 5. Dependence of microstructure of lamella-forming diblock copolymers on the confinement dimension d for the surfaces preferential to the minority blocks. The microstructures are arranged as d where the value of d and the structure denotations are list.

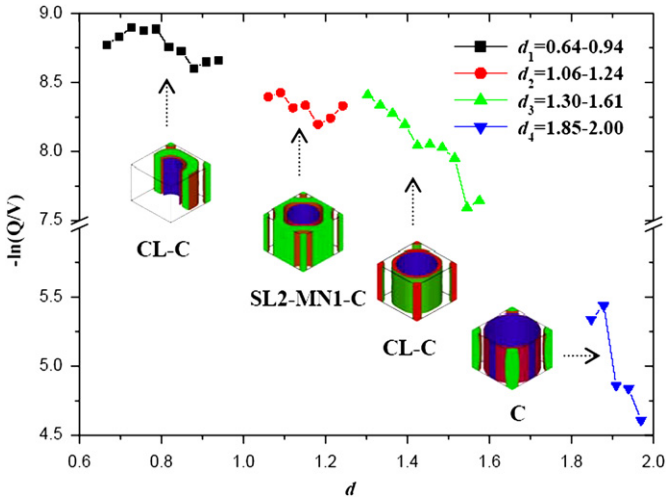

Fig. 6. The dependence of entropic free energy $-\ln(Q/V)$ on confinement dimension d for the surfaces preferential to the minority blocks. Four types of cylindrical microstructures and their denotations are shown in the corresponding positions. The dots denote the values of $-\ln(Q/V)$ for different d, while the simple lines are connected between two neighboring dots in order to observe their variations.

of the entropy effects. At $d = 0.52$, we observed the CL–PAL mixture structure for the preferential surface, similar to the neutral surface case in Fig. 2a2. Unlike the neutral surface case where the hard wall effect leads to the CL structure in the inner zone, the preferential surface requires that the majority blocks segregate surrounding the surfaces to form the CL structure [Fig. 4a4]. Furthermore, the BN2, PEL and CL–PAL structures were observed at a very narrow range of d, reflecting that these microstructures are sensitive to the confinement dimension.

There are three types of microstructures appearing in the second stage of $d_2 = 0.58$–1.00. At $d = 0.58$–0.76, the diblock copolymers are assembled into another complicated microstructure, which is similar to those observed in Fig. 4a2 and b1. From the side views of structures for the different domains, it is an evidence that this microstructure is a bicontinuous (BN3) structure. Accompany with this BN3 structure in the outer zone, there is a ring structure appearing in the inner zone so that we defined this structure as the bicontinuous network and ring mixture structure (BN3-R structure). Then, the microstructure develops into another complicated microstructure at $d = 0.82$–0.88 [Fig. 4b2]. As a whole, it is still a mixture structure with the bicontinuous network (BN4) and a ring structure, except that the unperfected cylinders embedded in the outer zone corner (that is, the BN4-R-C structure). It is interesting that the bulk PAL structure emerges at $d = 0.94$–1.00, reflecting that the confinement-dimension effect counteracts the surface field effect at this range of d [Fig. 4b3].

For the third stage of $d_3 = 1.06$–1.42, it starts with a bicontinuous network (BN5) structure in the outer zone at $d = 1.06$. However, the slit view shows that the ring structure disappears in the inner zone as the d increases [Fig. 4c1]. With increasing d, we observed the complex structure at $d = 1.12$–1.24 [Fig. 4.c2]. In this structure, it is difficult to distinguish the inner and outer zones because the structure is a bicontinuous network (BN6) structure in the whole zone, similar to the outer structure in Fig. 4b2. Then, the structure evolves into the PAL structure once again at $d = 1.30$–1.42 due to the similar reason explained in Fig. 4b3. For $d_4 = 1.48$–2.00, since the rod occupy much space in the array and the inner structure is difficult to assemble in the array. Furthermore, it is easy to assemble the sphere structure in the outer zone. For example, there is sphere-like (S3) structure appearing in the outer zone except that the unperfected lamella (UL) structure, namely the UL-S3 structure occurs at $d = 1.48$–1.55 [Fig. 4d1]. With increasing d, the UL structure develops into a bicontinuous network (BN7) structure at $d = 1.61$–1.85 [Fig. 4d2]. For the larger d, the disperse structure can also be observed under this condition instead of the PAL structure. The example is that the sphere-like (S4) structures were observed at $d = 1.90$–2.00 [Fig. 4d3].

It is worthwhile to conclude the general characteristic of structures observed in these four stages. The first characteristic is that the PAL structure occur in the ends of the first three stages, namely for $d = 0.52$, $d = 0.94$–1.00 and $d = 1.30$–1.42, which is nearly equal to the half integers. This is possibly due to the balance between the surface field and the confinement dimension that had not been observed in the previous work where the confinement dimension varies over a narrow range [39]. The second characteristic is that the complicated microstructures always with the majority blocks congregating surround the rod surfaces. In the nanopore-confinement, the results also show that there are asymmetric in the phase diagram where the more complicated microstructures can be observed when the surface prefers to the majority blocks [19]. Since the surface prefers to the majority blocks, leading to an obvious adsorption effect for this block, the alteration for the surface domain come into being a series of complicated microstructures in the array. Furthermore, although the surface field is cylindrical, the cylinder structure almost does not appear because of the weak surface field.

However, this is not the case for the strong surface field. Therefore, we investigated the microstructures at strong surface field of $U_A = -40$ in Fig. 5. Similar to the neutral case, the evolvement process can also be divided into three stages, the $d_1 = 0.03$–0.57, $d_2 = 0.64$–1.24, and $d_3 = 1.30$–2.00 stages. For the stage of $d_1 = 0.03$–0.57, we observed the CL–PAL mixture structure at $d = 0.03$–0.15 where there is a CL structure in the inner zone and a PAL structure in the outer zone [Fig. 5a1]. Unlike the neutral case where the hard wall effect lead to the CL structure in the inner zone, the preferential surfaces result in the CL structure in this case. Then, a complicated structure, the mono-continuous network (MN4), mesh (M) and CL mixture structure (MN4-M-CL structure), appears at $d = 0.21$, due to the strong adsorption effect from the surfaces [Fig. 5a2]. At $d = 0.27$–0.57, this effect requires the diblock copolymers keep the CL–LN structure, similar to the microstructure observed in the neutral surface at $d = 0.33$–0.45 [Fig. 5a3]. One difference is that the former has a slightly wider range than the latter, due to the strong adsorption between the surface and minority blocks. At the second stage of $d_2 = 0.64$–1.24, the strong adsorption effect eliminates the non-cylindrical structure in the process so that the CL structure occurs in the inner zone while the C structures in the outer zone, [Fig. 5b1–b3]. For example, the perfect CL structure can be observed in the inner zones at $d = 0.64$–0.94, while the cylinder structure occurs in the outer zone for the whole intermediate stage, that is, the CL-C structure at the minority block domain. This fact is similar the case of the cylindrical nanopore-confinement, in which the strong cylindrical surface field also lead to the CL structure that observed in the MC simulations [4,20], the DDFT simulations [15] and experiments [16,49]. However, we note that the outer structure at $d = 1.00$ have slightly irregular cylindrical symmetry, that is a bicontinuous network (BN8) structure, which can be explained as the symmetric conflict between the inner and outer zones. Therefore, we observed a BN8-C structure at $d = 1.00$ that develop into an SL2-MN1-C structure at $d = 1.06$–1.24. The SL2-MN1-C structure has a wider range of d than that observed in Fig. 2b4 because of the strong adsorption surface field. Then, we investigated the lager d case of $d = 1.30$–2.00 [Fig. 5c1–c4]. The MN2 structure maintains a wider range of $d = 1.67$–1.79 than that observed at Fig. 2c1 in the neutral surface case because the strong

surface field attracts the minority blocks and makes it difficult to transit into the other structure. The only non-cylindrical structure occurs at $d = 1.79$ where the sphere-like (S5) structure embedded at majority block matrix in the outer zone [Fig. 5c3]. For the whole evolvement process, it was demonstrated that the structures exhibit more cylindrical symmetry than those observed in the neutral case because of the strongly cylindrical surface fields. For example, at $d = 1.91$–2.00, the diblock copolymers exhibit a sphere-like structure in the neutral case, while these non-cylindrical structures come into being the C structures in the outer zone in the strong surface field case.

The cylinder structure is a popular structure that not only appears in the case of neutral surfaces but also in those of preferential surfaces in the outer zone. Here, we discuss these structures by comparing their entropic free energies. According to Eq. (1), we obtained the entropic free energies $-\ln(Q/V)$ for different equilibrium structures, and plotted the dependence of $-\ln(Q/V)$ on the d for the surface preferential to the minority blocks in Fig. 6. It is clear that $-\ln(Q/V)$ decreases with increasing d in the whole process. This can explained that the confinement space decrease as the d increases so that the entropy loss increases. The entropy loss is most obvious for the case of $d_4 = 1.85$–2.00, in which the diblock copolymers have the cylinder structure. In general, the entropic energy, $-\ln(Q/V)$, almost has the similar variations with the increasing of d in the other three cases, namely the cases of $d_1 = 0.64$–0.94, $d_2 = 1.06$–1.24, and $d_3 = 1.30$–1.61. The smooth variation in each case indicates that there is no first-order phase transition in each process. In fact, there is not abrupt structural transition in each case other than the transitions in different cases.

4. Conclusion

In this paper, we have performed SCFT calculations to investigate the microstructures of lamella-forming diblock copolymers confined in the nanorod arrays with neutral surfaces and preferential surfaces, respectively. We chose the model copolymers to be slightly asymmetric diblock copolymers in the relatively strong segregation region, while the period of nanorod array is chosen to be three times as the bulk lamella period. Under these considerations, we have observed a rich variety of the microstructures in the arrays with the neutral and preferential surfaces by varying the fractional confinement-dimension, respectively.

For the arrays with neutral surfaces, a rich variety of mixture microstructures of the diblock copolymers have been observed by varying the fractional confinement-dimension. For the small d, the mixture structures display the lamellar characteristic, such as the PAL and CL–LN structures. However, there are the cylindrical structures in the outer zone at the moderate d including the SL1-C, NCL-C, SL2-BN1-C, SL2-MN1-C and CL-C mixture structures. At the large d, the discrete structures like the S and GC structures occur in the outer zone. These mixture structures have been compared to the available simulations and experiments, which can be explained based on the symmetry competition between the inner and outer zones, as well as the structural frustration. It is believed that the fractional confinement-dimension is crucial to determine the microstructures through influencing either the symmetry competition or the structural frustration. Furthermore, the dependence of the minimal free energies on the equilibrium microstructures was used to analyze the structural transition behaviors in the small, moderate and large d cases. The results indicate that the outer structure transition plays an important role in the evolvement process. The diblock copolymers have the different evolution trends in the small, moderate and large d cases, reflecting that there is a first-order phase transition in the whole process when the structure changes obviously.

On the other hand, we have investigated the microstructures of lamella-forming diblock copolymers in the case of preferential surfaces by varying the fractional confinement-dimension. For the surfaces preferential to the majority blocks, the weak surface field can induce a series of continuous network structures including the BN2, BN3-R, BN4-R-C, BN5, and BN6 structures. The outstanding characteristic is that the PAL structure has been observed periodically with the given confinement-dimensions because of the compromise between the surface field and the confinement-dimension. For the surfaces preferential to the minority blocks, the strongly cylindrical surface field requires the microstructures with the cylindrical symmetry, such as the CL-C, BN8-C and MN2-C structures, where a relatively simple evolvement process has been observed. It should be pointed out that the discrete microstructures appear in the severe confinement degree, namely the large d, for both cases. Moreover, the entropic energies for cylinder structures have been investigated, in order to illustrate the structural behaviors of these structures. In the preferential surface case, we also compared our results to the available simulations and experiments, as well as our previous work, which are in a general agreement.

Acknowledgments

This research was supported by the General Program of National Natural Science Foundation of China (Nos. 20574052, 20774066, 90403022, and 20804001), the Outstanding Youth Fund of China (No.20525416), and the National Basic Research Program of China (No.2005CB623800).

References

[1] Urbas A, Sharp R, Fink Y, Thomas EL, Xenidou M, Fetters LJ. Adv Mater 2000; 12:812.
[2] Urbas A, Thomas EL, Kriegs H, Fytas G, Penciu RS, Economou LN. Phys Rev Lett 2003;90:108302.
[3] Yoon J, Lee W, Thomas EL. Nano Lett 2006;6:2211.
[4] Yu B, Sun P, Chen T, Jin Q, Ding D, Li B, Shi A-C. J Chem Phys 2007;126:204903.
[5] Xiang H, Shin K, Kim T, Moon S, McCarthy TJ, Russell TP. J Polym Sci Part B 2005;43:3377.
[6] Lambooy P, Russell TP, Kellogg GJ, Mayes AM, Gallagher PD, Satija SK. Phys Rev Lett 1994;72:2899.
[7] Koneripalli N, Singh N, Levicky R, Bates FS, Gallagher PD, Satija SK. Macromolecules 1995;28:2897.
[8] Pickett GT, Balazs AC. Macromolecules 1997;30:3097.
[9]. Matsen MW. J Chem Phys 1997;106:7781.
[10] Geisinger T, Muller M, Binder K. J Chem Phys 1999;111:5241.
[11] Wang Q, Yan Q, Nealey PF, De Pablo JJ. J Chem Phys 2000;112:450.
[12] Xu T, Hawker CJ, Russell TP. Macromolecules 2005;38:2802.
[13] Angerman HJ, Johner A, Semenov AN. Macromolecules 2006;39:6210.
[14] Alexander-Katz A, Fredrickson GH. Macromolecules 2007;40:4075.
[15] Sevink GJA, Zvelindovsky AV. J Chem Phys 2008;128:084901.
[16] Xiang H, Shin K, Kim T, Moon SI, McCarthy TJ, Russell TP. Macromolecules 2004;37:5660.
[17] Feng J, Liu H, Hu Y. Macromol Theory Simul 2006;15:674.
[18] Feng J, Ruckenstein E. Macromolecules 2006;39:4899.
[19] Li W, Wickham RA, Garbary RA. J Chem Phys 2006;39:806.
[20] Chen P, He X, Liang H. J Chem Phys 2006;124:104906.
[21] Yu B, Sun P, Chen T, Jin Q, Ding D, Li B, Shi A-C. J Chem Phys 2007;127:114906.
[22] Wang Q. J Chem Phys 2007;126:024903.
[23] Feng J, Ruckenstein E. J Chem Phys 2006;125:164911.
[24] Arsenault AC, Rider DA, Ttreault N, Chen JI-L, Coombs N, Ozin GA, Manners I. J Am Chem Soc 2005;127:9954.
[25] Yu B, Li B, Jin Q, Ding D, Shi A-C. Macromolecules 2007;40:9133.
[26] Higuchi T, Tajima A, Motoyoshi K, Yabu H, Shimomura M. Angew. Chem. Int. Ed. 2008;47:8044.
[27] Chen P, Liang H, Shi A-C. Macromolecules 2007;40:7329.
[28] Huinink HP, Van Dijk MA, Brokken-Zijp JCM, Sevink GJA. Macromolecules 2001;34:5325.
[29] Park I, Park S, Park H-W, Chang T, Yang H, Ryu CY. Macromolecules 2006;39:315.
[30] Tsarkova L, Knoll A, Krausch G, Magerle R. Macromolecules 2006;39:3608.
[31] Yang Y, Qiu F, Zhang H, Yang Y. Polymer 2006;47:2205.
[32] Wang Q, Nealey PF, De Pablo JJ. Macromolecules 2001;34:3458.
[33] Yu B, Sun P, Chen T, Jin Q, Ding D, Li B, Shi A-C. Phys Rev Lett 2006;96:138306.
[34] Li W, Wickham RA. Macromolecules 2006;39:8492.
[35] Yu B, Jin Q, Ding D, Li B, Shi A-C. Macromolecules 2008;41:4042.

[36] Xiang H, Shin K, Kim T, Moon SI, McCarthy TJ, Russell TP. Macromolecules 2005;38:1055.
[37] Chen P, Liang H, Shi A-C. Macromolecules 2008;41:8938.
[38] Cheng JY, Ross CA, Smith HI, Thomas EL. Adv Mater 2006;18:2505.
[39] Li S, Chen P, Wang X, Zhang L, Liang H. J Chem Phys 2009;130:014902.
[40] He L, Zhang L, Xia A, Liang H. J Chem Phys 2009;130:144907.
[41] Fredrickson GH, Ganesan V, Dorlet F. Macromolecules 2002;35:16.
[42] Yang S, Yan D, Shi A-C. Macromolecules 2006;39:4168.
[43] Matsen MW, Schick M. Phys Rev Lett 1994;72:2660.
[44] Drolet F, Fredrickson GH. Phys Rev Lett 1999;83:4317.
[45] Meng D, Wang Q. J Chem Phys 2007;126:234902.
[46] Benedicto AD, O'Brein DF. Macromolecules 1997;30:3395.
[47] Wohlgemuth M, Yufa N, Hoffman J, Thomas EL. Macromolecules 2001;34:6083.
[48] He L, Zhang L, Liang H. J Phys Chem B 2008;112:4194.
[49] Shin K, Xiang H, Moon SI, Kim T, McCarthy TJ, Russell TP. Science 2004;306:76.